Morphology Development and Crystallization Behavior of a Poly(ethylene terephthalate)/Polycarbonate Blend

Jong Kwan Lee, Jeong Eun Im, Jong Hwan Park, Hong Youn Won, Kwang Hee Lee

Center for Advanced Functional Polymers, Department of Polymer Science and Engineering, Inha University, Incheon 402-751, Korea

Received 28 December 2004; accepted 15 March 2005
DOI 10.1002/app.22739
Published online 7 December 2005 in Wiley InterScience (www.interscience.wiley.com).

ABSTRACT: The morphology development and crystallization behavior of an extruded poly(ethylene terephthalate)/polycarbonate blend were studied with optical microscopy, light scattering, and differential scanning calorimetry (DSC). During annealing at 280°C, liquid–liquid phase separation via spinodal decomposition proceeded in a melt-extruded specimen. After the formation of the domain structure, the blend slowly underwent phase homogenization by transesterification between the two polymers. The specimen, annealed for various times (t_s's) at 280°C, was subjected to a temperature drop to 180°C for the isothermal crystallization, and then the effects of liquid-phase changes on crystallization were investigated. The crystal growth rate decreased with t_s. The slow crystallization with a large t_s value was associated with the composition change of the separated phases and the change of the sequence distribution in the polymer chains during annealing. The influence of t_s on the endothermic behavior of the samples was examined. As t_s increased, the recrystallization rate was retarded during the DSC scan, displaying multiendothermic behavior. The DSC data also suggested that the increased level of transesterification would give rise to a higher number of species being rejected from the primary crystals, leading to enhanced secondary crystallization. © 2005 Wiley Periodicals, Inc. J Appl Polym Sci 99: 2220–2225, 2006

Key words: crystallization; phase separation; polycarbonates

INTRODUCTION

It is well known that the morphology of crystalline polymer blends is highly influenced by the phase behavior in the molten state.[1–6] If the blend has a lower critical solution temperature (LCST) or upper critical solution temperature (UCST) phase diagram, crystallization may proceed simultaneously and compete with liquid–liquid (L–L) phase separation.[2,3,7] The two competitive processes may create unique morphological patterns that are not attainable by either process alone.

Blends of poly(ethylene terephthalate) (PET) and polycarbonate (PC) are basically immiscible over a wide range of compositions. During melt processing, a kind of reaction called transesterification takes place.[8–12] The reaction leads to the formation first of block copolymers and then of random copolymers, which enhance the miscibility of the blends.[13–16] With an increase in the reaction extent, the compatibility of the blends increases from complete incompatibility to partial compatibility and then to complete compatibility. Therefore, PET/PC blends can be expected to provide a nice opportunity for investigating the effects of various liquid-phase changes on crystalline morphology.

In this work, we carried out optical microscopy (OM) observations to confirm L–L phase separation via spinodal decomposition (SD) in an extruded PET/PC blend and investigated the effects of L–L demixing and subsequent phase homogenization on crystallization. The characteristics of the melting behavior were also examined on the basis of the effects of combined crystallization and L–L demixing.

EXPERIMENTAL

Materials

Commercial PET [weight-average molecular weight (M_w) = 52,000, weight-average molecular weight/number-average molecular weight (M_w/M_n) = 2.0], produced by Honam Petrochemical Co. (Seoul, Korea), was used. Bisphenol A polycarbonate (M_w = 36,000, M_w/M_n = 1.71) was obtained from Samyang Co. (Seoul, Korea). After being dried in a vacuum oven at 150°C for 24 h, PET and PC were melt-mixed at 280°C on a 30-mm corotating twin-screw extruder (Werner Pfleiderer, Frankfurt, Germany) at 200 rpm. The residence time for the melt mixing was less than 1 min. The extrudate was quenched in ice water to freeze the structure in the melt and was then chopped

Correspondence to: K. H. Lee (polylee@inha.ac.kr).
Contract grant sponsor: Inha University.

into pellets. The composition of the blend was 50/50 by weight.

Light scattering (LS) and OM

A thin-film specimen (ca. 15 μm thick) was prepared by the pressing of the pellets between two cover glasses at 280°C. Immediately after the melt pressing, the specimen was transferred onto a hot stage set at 280°C and was then annealed for a certain time (t_s). After that, the specimen was rapidly transferred onto an LS hot stage set at a desired crystallization temperature, and the effects of L–L phase separation and homogenization on crystallization were examined. A polarized He–Ne gas laser with a 632.8-nm wavelength was applied to the film specimen. We used the H_v geometry, in which the optical axis of the analyzer was set perpendicular to that of the polarizer. The final morphology of the crystallized specimen was also observed with OM.

Solubility testing

The pellets were compression-molded between metal plates at 280°C for t_s. After molding, the specimen was quenched in ice water to prevent crystallization. The amorphous specimen was treated with dichloromethane. In dichloromethane, the selective solvent used in this work, PC is soluble, and PET is not. Soluble and insoluble fractions in dichloromethane were separated, dried, and weighed.

Differential scanning calorimetry (DSC)

The thermal analysis was carried out with a TA Instruments 2920 DSC instrument (New Castle, DE) equipped with an intracooler. The glass-transition temperature (T_g) was defined as the midpoint of the heat capacity jump on DSC thermograms. The melting temperature and crystallization temperature were considered the maximum points of the endothermic and exothermic peaks, respectively. All measurements were performed at a heating rate of 10°C/min in a nitrogen atmosphere.

RESULTS AND DISCUSSION

L–L phase separation and homogenization

The occurrence of L–L phase separation and homogenization during annealing can be demonstrated by the morphology observed by OM. Figure 1 shows the morphological development of the PET/PC blend annealed at 280°C. In the beginning [Fig. 1(a)], a high level of interconnectivity in both phases can be seen, and the phases are regularly spaced. A two-phase structure with unique periodicity and phase connectivity is one of the hallmarks of SD. At the later stage of L–L phase separation [Fig. 1(b)], phase connectivity grows and eventually breaks up into a macroscopic spherical texture. These are characteristics of the SD mechanism. As the transesterification reaction proceeds, the domain growth is suppressed, and the blend morphology is mainly controlled by the phase homogenization process [Fig. 1(c)]. Finally, the blend shows a homogeneous mixture [Fig. 1(d)]. Supplementary evidence for L–L phase separation and homogenization may be provided through time-resolved light scattering (TR-LS). Unfortunately, in this system, no effective information was obtained from TR-LS because of the very small difference in the refractive indices of the constituent polymers.

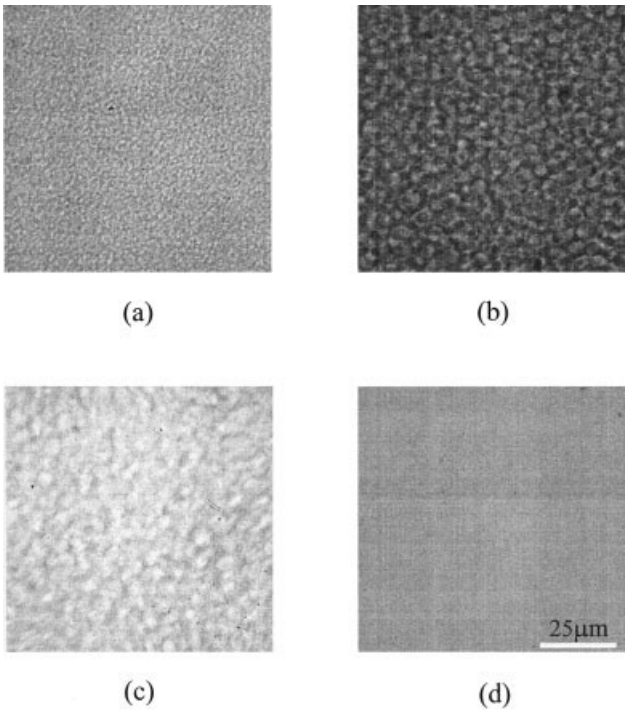

Figure 1 Optical micrographs of the PET/PC blend after annealing at 280°C for (a) t_s = 1 min, (b) t_s = 3 min, (c) t_s = 10 min, and (d) t_s = 15 min.

Figure 2 shows polarized optical micrographs for stepwise crystallized samples. The sample was first annealed between two cover glasses at 280°C for t_s and was then quenched in ice water to freeze the two-phase morphology. After that, the sample was isothermally crystallized at 120°C for 10 h. Because the crystallization temperature, 120°C, is below the T_g of PC, the crystallization mainly occurs in the PET-rich phase within the time period investigated. The crystallization causes the birefringence change in the PET-rich phase, enhancing the optical contrast between the separated phases. The contrast increases up to t_s = 3 min and then gradually decreases. The increase in contrast should be ascribed to the growth of the concentration

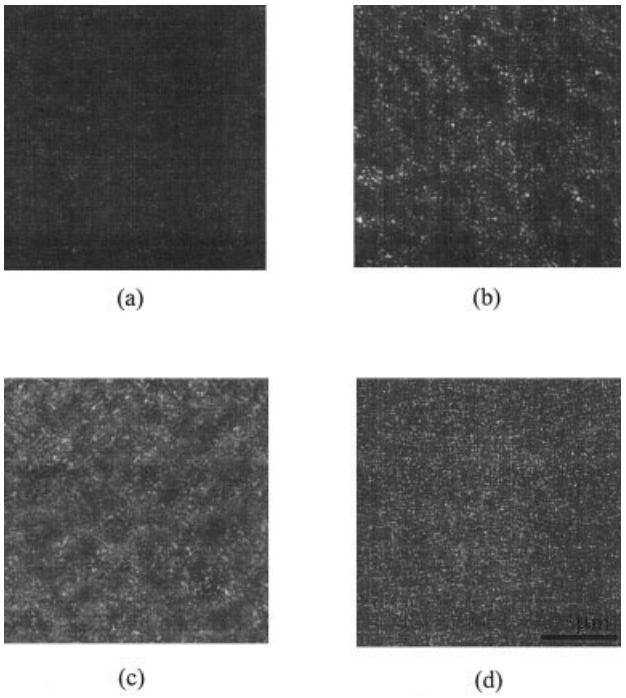

Figure 2 Polarized optical micrographs of the PET/PC blend crystallized at 120°C for 10 h after annealing at 280°C for (a) t_s = 1 min, (b) t_s = 3 min, (c) t_s = 10 min, and (d) t_s = 15 min.

fluctuation by SD, whereas the decrease suggests that the phase homogenization proceeds slowly in the later stage of annealing. A question raised by these results is why the demixing and domain growth occur first and the phase homogenization follows. It may be that the rate of SD is much faster than the rate of the transesterification reaction.

T_g may provide useful information on blend miscibility. For an immiscible blend, two T_g's generally appear on the DSC scan, whereas for miscible blends or copolymers, only one T_g is observed. In PET/PC blends, the cold crystallization of PET occurs in the same temperature range as the glass transition of PC. To distinguish the glass transition of PC from the cold crystallization of PET, the blend samples were isothermally crystallized at 120°C for 10 h before the DSC measurements. Figure 3 shows the change in T_g as a function of t_s. Double glass transitions for the sample of t_s = 1 min indicate that the blend has a two-phase structure with a certain concentration fluctuation in the beginning. Because the concentration fluctuation between the separated phases increases in the early stage of annealing ($t_s < 3$ min), the inward shift of the T_g's for the t_s = 3 min sample may appear contradictory. The PET–PC copolymer species, which have an intermediate T_g in comparison with the pure polymers, might be formed in the early stage of annealing even though their effects on the phase dissolution were not observed under OM. Therefore, the inward

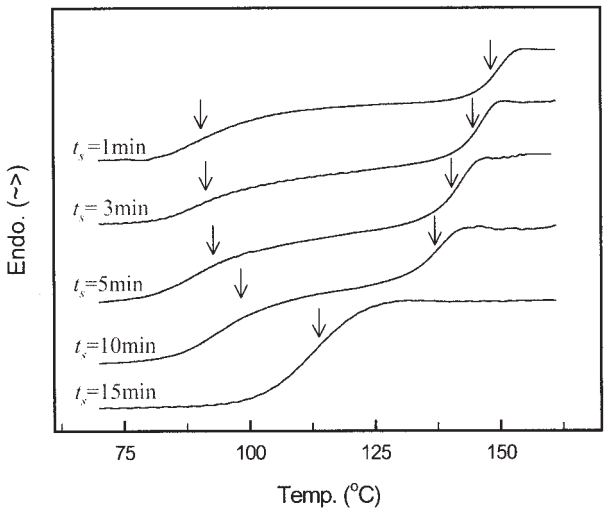

Figure 3 Change in T_g with t_s (T_g is indicated by the arrows).

shift of the T_g's implies that the T_g behavior of the PET/PC blend would be highly dependent on the formation of the PET–PC copolymer species by the transesterification of the two polymers as well as the change in the concentration fluctuation between the separated phases. As t_s increases, the T_g's approach toward each other, and finally a single glass transition is observed. This indicates that the level of transesterification between the two polymers increases with t_s, leading to the formation of a single amorphous phase. The increase in the heat capacity jump with t_s suggests that morphological homogeneity is enhanced through the phase homogenization process.

Figure 4 shows the DSC thermograms of the blend samples quenched after annealing at 280°C for t_s. The cold-crystallization peak temperature shifts to a

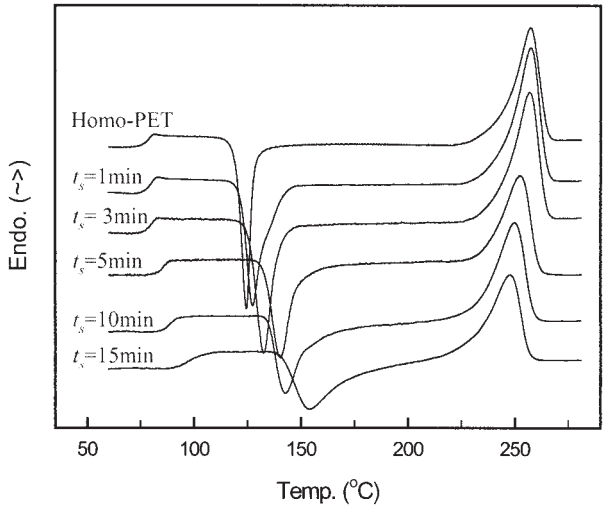

Figure 4 DSC heating thermograms of various samples quenched after annealing at 280°C for t_s.

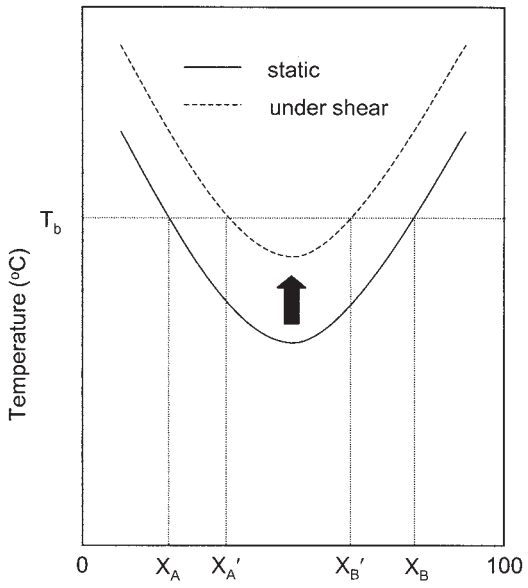

Figure 5 Schematic drawing of the change in the phase diagram with the shear rate. The arrow indicates the elevation of T_s at a high shear rate.

higher temperature, and the peak width increases with t_s. This indicates that the PET crystallization is significantly affected by the change in the sequence distribution in the polymer chains and the composition change between separated phases. The melting temperature and the melting peak area decrease with t_s as expected.

On the basis of these results, it can be concluded that the structure development of the extruded PET/PC blend in the early stage of annealing is dominated by the SD mechanism. A possible explanation for this phase behavior may be given as follows: at high shear rates in the extruder, the spinodal temperature (T_s) in the LCST phase diagram may be elevated, as shown by the arrow in Figure 5, and the one-phase region becomes wider. Thus, the system undergoes phase dissolution. The dissolution continues until a new composition is reached in the mixture. The compositions X_A and X_B at a static condition move to the compositions X_A' and X_B' in the shear field. This could be the case for this PET/PC blend. If T_s in the shear field is raised above the barrel temperature (T_b), the mixing can be done in a one-phase region to obtain a homogeneous mixture. The phase diagram in Figure 5 is just a schematic illustration and does not have any quantitative significance; it indicates that the mixture is thermodynamically unstable. It is conceivable that the blend may not have an LCST phase diagram but rather has an UCST phase diagram. In that case, T_s in the shear fields should be lowered to induce the dissolution of the components. Once the melt is extruded from the nozzle, the shear rate turns to zero and T_s immediately falls to a static value, so SD proceeds until the structure is fixed by being cooled down below the T_g's of the components. The freezing chain mobility at a low temperature prevents further L–L phase separation.

Solubility testing

Figure 6 shows the change in the soluble weight fraction with t_s. In the absence of any interchange reactions, the soluble weight fraction for the blend may remain constant at 50 wt %. On the other hand, when interchange reactions take place, a progressive shift toward larger amounts of the soluble or insoluble fraction is expected because the copolymers formed by transesterification have a different solubility on account of the dominance of PET or PC blocks. The initial decrease in the solubility implies that PET is incorporated into the intramolecular part of PC, leading to the formation of block copolymers. The large increase in the soluble fraction for $t_s > 30$ min can be attributed to the shortening of the average block length. The crystallizable sequence lengths of the PET–PC copolymers would be long enough to participate in the crystallization for the samples investigated in this work.

Crystallization

To discuss crystallization, it is convenient to use the LS invariant in the H_v mode, Q_{Hv}. Q_{Hv} is proportional to the mean-square optical anisotropy, $\langle\delta^2\rangle$:

$$Q_{Hv} \propto \langle\delta^2\rangle = \phi_s \delta_s^2 \tag{1}$$

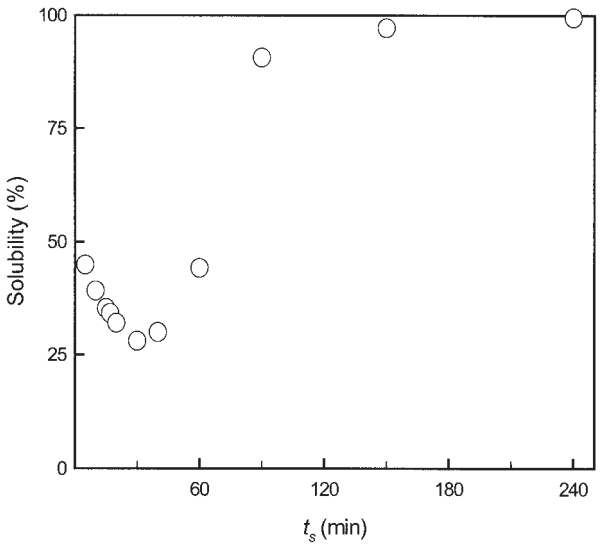

Figure 6 Solubility in dichloromethane for the PET/PC blend after annealing at 280°C for t_s.

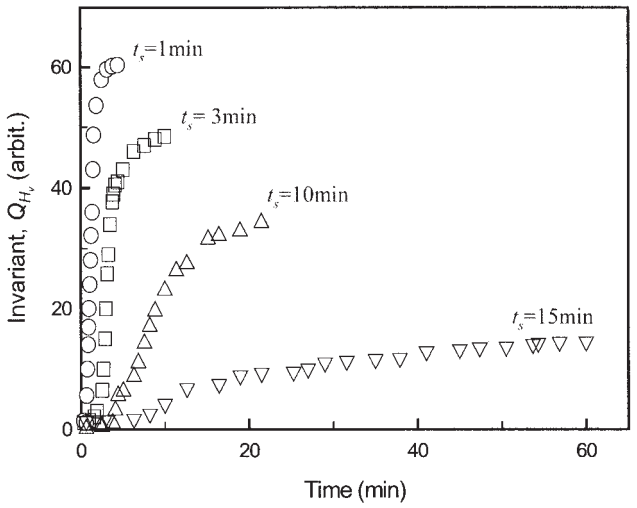

Figure 7 Time variation of Q_{Hv} for the PET/PC blend crystallized at 180°C after annealing at 280°C for t_s.

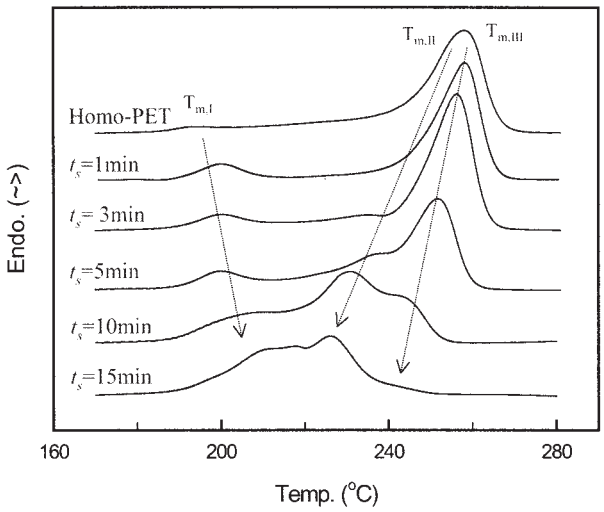

Figure 9 DSC thermograms of various samples crystallized isothermally at 180°C for 4 h. Pure PET first was melted at 280°C for 5 min and then was crystallized. The blend samples were crystallized after annealing at 280°C for t_s.

where ϕ_s is the volume fraction of spherulites and δ_s is the spherulite anisotropy.[17]

The time variations of Q_{Hv} during crystallization at 180°C after t_s = 1, 3, 10, and 15 min are shown in Figure 7. Q_{Hv} increases with time and then levels off as expected from eq. (1); that is, ϕ_s increases and attains a maximum value when spherulites fill the whole space. Q_{Hv} is assumed to be proportional to ϕ_s, so the linear growth rate of the spherulite (G) is

$$G \propto d[Q_{Hv}(t)/Q_{Hv}(\infty)]^{1/3}/dt \quad (2)$$

where $Q_{Hv}(\infty)$ is the attainable invariant at a given crystallization condition. Therefore, one can estimate G from the slope of the time variation of $[Q_{Hv}(t)/Q_{Hv}(\infty)]^{1/3}$. G, estimated by eq. (2), is shown as a function of t_s in Figure 8. G decreases with t_s, and this indicates that the crystallization of PET is significantly hindered because of the disruption of chain periodicity as a result of transesterification. The increasing T_g of the PET-rich phase with t_s reduces the chain mobility of PET, so the crystallization rate is further retarded.

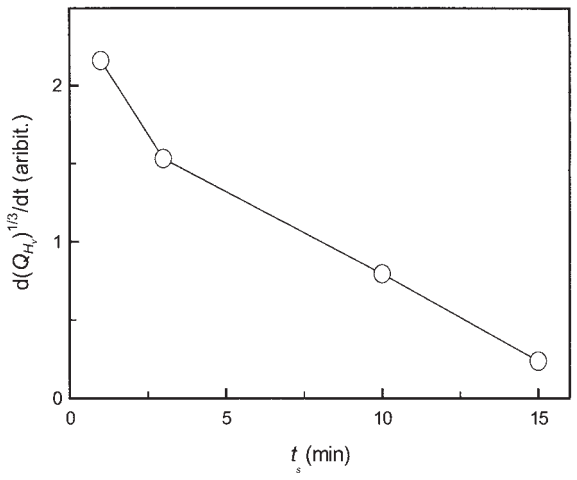

Figure 8 Change in G with t_s.

Figure 9 shows DSC thermograms of various samples crystallized isothermally at 180°C for 4 h after annealing at 280°C for t_s. The crystallization temperature of 180°C was chosen on the basis of our knowledge of the rapid growth rate of PET crystals. Conceptually, it seems plausible that the rapid crystallization of PET at 180°C is very effective for locking in further growth of the L–L phase separation. Both the pure PET and the blend samples exhibit multiple-melting endotherms. Various models have been proposed to explain this behavior. The two primary models are (1) the melting and recrystallization model and (2) the dual population of lamellar thickness model. One of the most recent studies on the multiple-melting behavior of PET based on DSC was reported by Al Raheil.[18] He used a combination of the melting–recrystallization model and the dual lamellar population model to explain the triple-melting behavior. The three melting endotherms were denoted peaks I, II, and III in order of the melting point, respectively. The lowest melting peak ($T_{m,I}$) was attributed to melting of the subsidiary lamellae formed by secondary crystallization. The second ($T_{m,II}$) was associated with melting of the dominant lamellae. The third melting peak ($T_{m,III}$) was assigned to melting of the crystals formed by a reorganization process during the DSC scan. Several interesting features can be seen in the figure. With increasing t_s, the $T_{m,II}$ and $T_{m,III}$ peaks are split, and their positions shift to lower temperatures. The peak

area of $T_{m,II}$ increases with t_s, whereas the $T_{m,III}$ peak decreases and finally disappears for a prolonged annealing. Modulated differential scanning calorimetry (MDSC) is a new thermal analysis tool that enables the separation of a seemingly single peak resulting from overlapping multiple thermal events over similar temperature ranges into two or more independent peaks. With MDSC, it was confirmed that the peaks of $T_{m,II}$ and $T_{m,III}$ were overlapped for the samples of $t_s < 3$ min (data not shown). In the pure PET, melting and subsequent recrystallization of primary crystals occur at the same time, so the two melting peaks merge together. Up to $t_s = 3$ min, the melting behavior of the blend is similar to that of pure PET. As t_s increases, the chain regularity and the mobility of the PET components decrease because of the homogenization process via transesterification. As a result, the recrystallization rate is gradually retarded during the DSC scan, and this leads to the spilt of the two independent peaks, $T_{m,II}$ and $T_{m,III}$. For the sample of $t_s = 15$ min, the recrystallization is largely restricted, so the peak of $T_{m,III}$ appears as a weak shoulder in the DSC trace. Another important characteristic of the DSC traces is that the $T_{m,I}$ peak is strongly enhanced with t_s. As mentioned previously, the $T_{m,I}$ peak is related to the secondary crystallization of species rejected from the primary crystals. Therefore, it can be speculated that the increasing level of transesterification would give rise to a higher number of species being rejected from the main crystals, and as a result, an increase in the secondary crystallization would occur.

CONCLUSIONS

We studied the morphological changes and subsequent crystallization behavior in a PET/PC blend. On the basis of the results described in this article, we were able to make the following conclusions:

1. The L–L phase separation occurred during annealing. After the formation of the domain structure, the blend slowly underwent homogenization by transesterification between the two polymers.
2. The crystallization rate of the PET components was significantly affected by the composition change of the separated phases and the change of the sequence distribution in the polymer chains determined by the level of transesterification.
3. The incorporation of PC moieties into the intramolecular part of PET seemed to cause enhanced secondary crystallization.

This research was supported by Inha University Research Grant. Synchrotron small-angle X-ray scattering experiments were performed at the Pohang Light Source (4C1 beam line) in Korea.

References

1. Chen, H. L.; Hsiao, M. S. Macromolecules 1998, 31, 6579.
2. Inaba, N.; Sato, K.; Suzuki, S.; Hashimoto, T. Macromolecules 1986, 19, 1690.
3. Inaba, N.; Yamada, T.; Suzuki, S.; Hashimoto, T. Macromolecules 1988, 21, 407.
4. Chen, H. L.; Hwang, J. C.; Yang, J. M.; Wang, R. C. Polymer 1998, 39, 6983.
5. Nojima, S.; Satoh, K.; Ashida, T. Macromolecules 1991, 24, 942.
6. Okamoto, M.; Kotaka, T. Polymer 1997, 38, 1357.
7. Lee, C. H.; Saito, H.; Inoue, T. Macromolecules 1995, 28, 8096.
8. Kotliar, A. M. J Polym Sci Part D: Macromol Rev 1981, 16, 367.
9. Pilati, F.; Marianucci, E.; Berti, C. J. J Appl Polym Sci 1985, 30, 1267.
10. Godard, P.; Dekoninck, J. M.; Devleaver, V.; Devaux, J. J Polym Sci Part A: Polym Chem 1986, 24, 3301.
11. Godard, P.; Dekoninck, J. M.; Devleaver, V.; Devaux, J. J Polym Sci Part A: Polym Chem 1986, 24, 3315.
12. Montaudo, G.; Puglisi, C.; Samperi, F. Macromolecules 1998, 31, 650.
13. Suzuki, T.; Tanaka, H.; Nishi, T. Polymer 1989, 30, 1287.
14. Murff, S. R.; Barlow, J. W.; Paul, D. R. J Appl Polym Sci 1984, 29, 3231.
15. Kim, W. N.; Burns, C. M. J Polym Sci Part B: Polym Phys 1990, 28, 1409.
16. Wang, L. H.; Huang, Z.; Hong, T.; Porter, R. S. J Macromol Sci Phys 1990, 29, 155.
17. Okamoto, M.; Shiomi, K.; Inoue, T. Polymer 1995, 36, 87.
18. Al Raheil, I. A. M. Polym Int 1994, 35, 189.